Bumblebee Flight in Heavy Turbulence: Supplemental Material

T. Engels [1,2], D. Kolomenskiy[3], K. Schneider[1], F.-O. Lehmann[4] and J. Sesterhenn[2]

[1] *M2P2-CNRS & Aix-Marseille Université, 38 rue Joliot-Curie, 13451 Marseille cedex 20 France*
[2] *ISTA, Technische Universität Berlin, Müller-Breslau-Strasse 12, 10623 Berlin, Germany*
[3] *Graduate School of Engineering, Chiba University, 1-33 Yayoi-Cho, Inage-Ku, Chiba-Shi, Chiba 263-8522, Japan*
[4] *Department of Animal Physiology, Universität Rostock, Albert-Einstein-Strasse 3, 18059 Rostock, Germany*

I. SUPPORTING RESULTS

A. Detailed analysis of flight measures

In the following figures 1–3 we provide the time evolution of the lift force, aerodynamic power and pitch moment, for each independent wingbeat in the turbulent cases with $Tu = 0.17...0.99$ ($N_w = 16...108$). For comparison, the corresponding evolution in the laminar case is also shown, as well as the average profiles over all turbulent realizations for a given Tu. The latter two curves overlap significantly, illustrating that the ensemble-averaged wing force/moment/power is almost the same as in the laminar case for all times t/T, and not only its integral value.

B. Generalization of results: Supporting results for a different insect model

The results presented in the main text were obtained using the model bumblebee described below. However the results are expected to be generalizable to a wider range of flapping insects in a similar Reynolds number regime. The typical leading edge vortex has been observed even in bird flight, however our results are likely not applicable for very large flyers that might partially glide. For the smallest insects, the effect of ambient turbulence may be reduced to a quasi-steady large-scale perturbation.

To further support our results, we consider an additional insect model. It geometry is based on a fruitfly [10], the wingbeat kinematics is adapted from [7], where hovering flight was considered. The positional, feathering and elevation angle of the wing is visualized in figure 4 (right). Since [7] considered hovering flight, we increased the body pitch angle by $\beta = -15°$ and the stroke plane angle by $\eta = -45°$, as visualized in figure 4 (left). The body is thus more horizontal and the stroke plane is inclined with respect to the horizontal plane. The Reynolds number is set to $Re = 1296$, which is thus 10 times as high as for a fruitfly. We therefore refer to this model as a model housefly.

The model housefly is, unlike the model bumbblebee, not designed to mimic a real animal. Its purpose is rather to illustrate that the stability of the leading edge vortex in turbulent inflow is a generic feature, and not limited to the bumblebee. For this reason, we give all quantities in this subsection in dimensionless units, using R, f and ϱ_f as normalization.

Except the insect model, the free-stream velocity $u_\infty = 1.2$ and the viscosity $\nu = 1.16 \cdot 10^{-3}$, the setup is unaltered. The same resolution and time stepping is used, and likewise a series of runs with different turbulent inflow fields with the same statistical properties is performed. We fix the turbulence intensity to $Tu = 0.44$ (with $\Lambda = 0.771$, $\lambda = 0.220$, $\ell_\eta = 0.011$, $Re_\lambda = 100$, $N_R = 9$, $N_w = 36$).

As for the bumblebee in the main text, we first visualize the model in laminar inflow. Visual inspection of the $\|\underline{\omega}\| = 100$ isosurface in figure 5 reveals features similar to the bumblebee: a pronounced leading edge vortex is visible, connected to larger wingtip vortices. Owing to the reduced Reynolds number, the flow field presents less small scales then in the case of the bumblebee (see Movie S1).

To limit computational efforts, we study only one turbulence intensity for this model. Table I summarizes the results obtained in laminar and turbulent inflow.

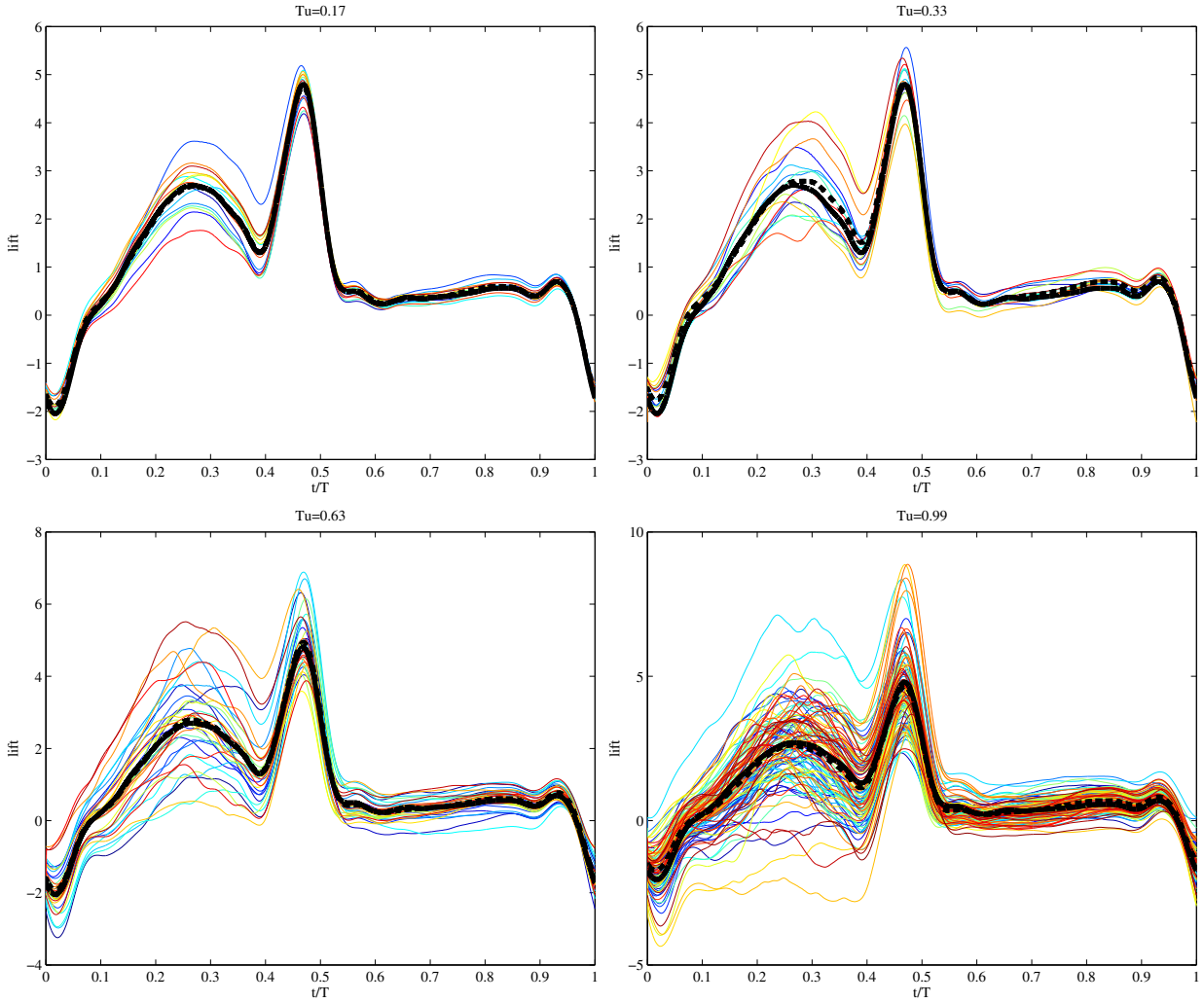

Figure 1. Lift force (normalized by weight force) as a function of wing beat fraction time t/T, for different values of $Tu = \{0.17, 0.33, 0.63, 0.99\}$. Thin colored lines represent individual realizations for the given turbulence intensity. The average over all turbulent realizations for the given Tu is represented by the thick black dashed line and the laminar case by the thick black continuous line. The averaged turbulent and laminar curves virtually coincide.

Tu	Forward force F_h	Vertical force F_v	Aerodynamic power P_{aero}	Moment M_x (roll)	Moment M_y (pitch)	Moment M_z (yaw)
0	-0.94	4.99	19.15	0.00	-0.69	0.00
0.44	$-1.05^{\pm 0.09} \pm 0.26$	$5.00^{\pm 0.15} \pm 0.46$	$19.18^{\pm 0.31} \pm 0.96$	$-0.01^{\pm 0.05} \pm 0.16$	$-0.70^{\pm 0.04} \pm 0.13$	$-0.04^{\pm 0.07} \pm 0.22$

Table I. Model housefly. Aerodynamic forces, power and moments obtained in the numerical experiments. All quantities are dimensionless (using R, f, ϱ_∞ as reference values). Values are given by mean value $\overline{x}$, 95% confidence interval δ_{95} and standard deviation σ in the form $\overline{x}^{\pm\delta_{95}} \pm \sigma$. Results were obtained by performing $N_R = 9$ simulations, yielding $N_w = 36$ statistically independent wingbeats.

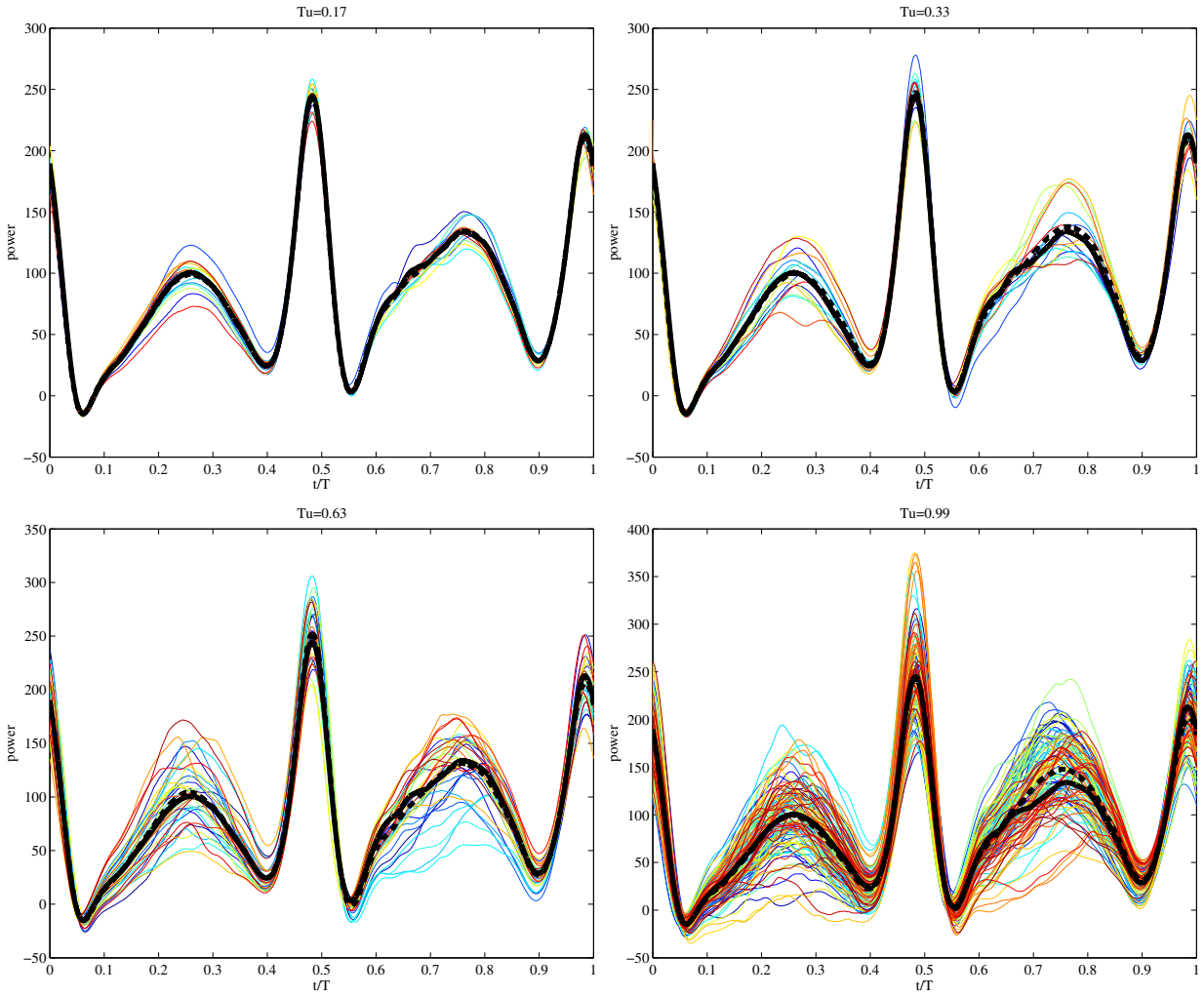

Figure 2. Aerodynamic power [W / kg body mass] as a function of wing beat fraction time t/T, for different values of $Tu = \{0.17, 0.33, 0.63, 0.99\}$. Thin colored lines represent individual realizations for the given turbulence intensity. The average over all turbulent realizations for the given Tu is represented by the thick black dashed line and the laminar case by the thick black continuous line. The averaged turbulent and laminar curves virtually coincide.

The conclusions from these simulations are similar to those drawn from the bumblebee. The average forces are not significantly different compared to the laminar case, and thus the underlying aerodynamic mechanisms are robust with respect to turbulent perturbations. Finally, we visualize in figure 6 the instantaneous lift force and aerodynamic power. Visibily, as in figures 1–3, the ensemble-averaged time series is in good agreement with the laminar curve.

II. MATERIALS AND METHODS

A. Model bumblebee

The parameters of the bumblebee model were derived from [4], case BB01. The animal's body mass, m, is approximately 175 mg and the wing length, R, amounts to 13.2 mm. We assumed the insect to be composed of linked rigid bodies and modeled the insect's body shape by sweeping an elliptical section of variable size along a curvilinear centerline. Compared to other insects, bumblebees have relatively thick legs that potentially create non-negligible aerodynamic effects. We thus included all legs, the proboscis and the antennae in our model as circular cylindrical sections joined by spheres, and further assumed bilateral

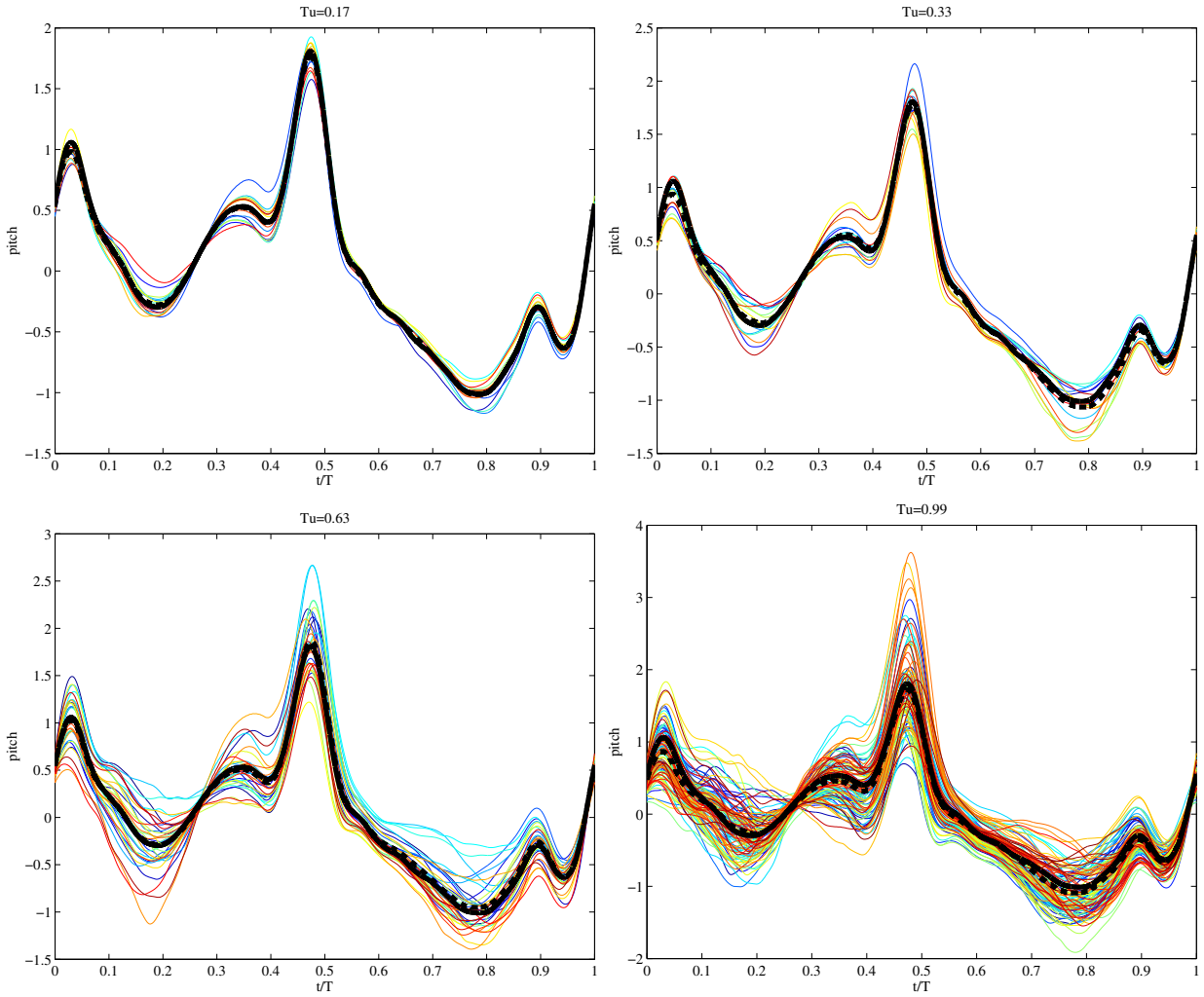

Figure 3. Pitch moment (normalized by weight force times wing length) as a function of wing beat fraction time t/T, for different values of $Tu = \{0.17, 0.33, 0.63, 0.99\}$. Thin colored lines represent individual realizations for the given turbulence intensity. The average over all turbulent realizations for the given Tu is represented by the thick black dashed line and the laminar case by the thick black continuous line. The averaged turbulent and laminar curves virtually coincide.

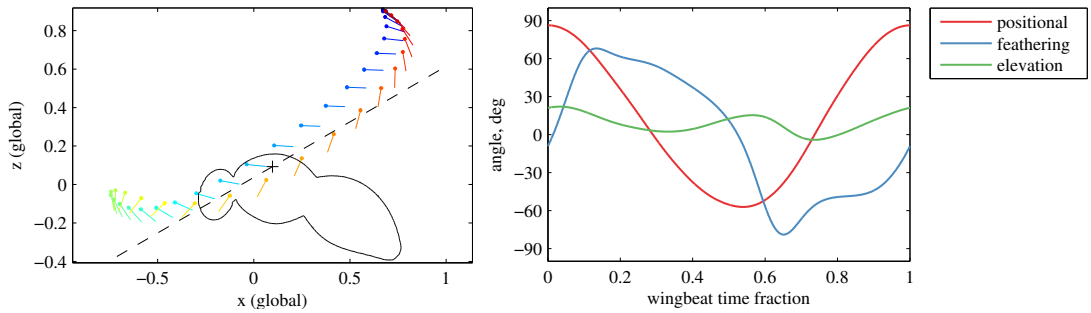

Figure 4. Morphology for the model housefly. Left: visualization of the wingbeat. Right: wingbeat kinematics as a function of t/T.

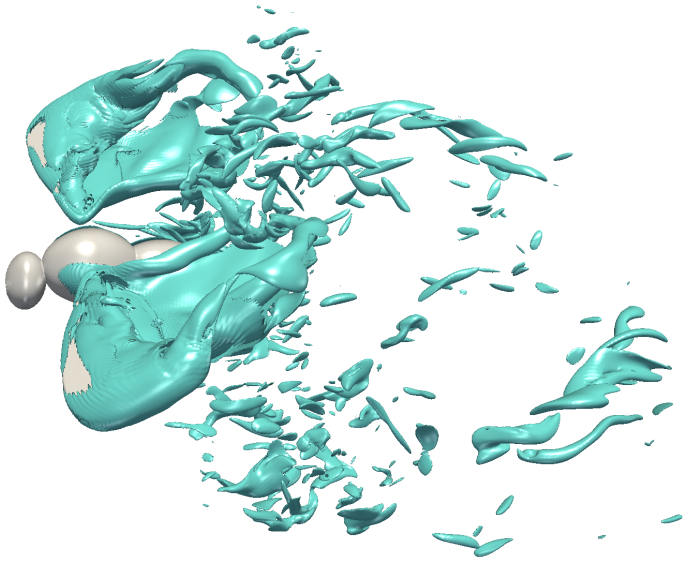

Figure 5. Flow field generated by the model housefly under laminar inflow condition. Shown is the $\|\underline{\omega}\| = 100$ isosurface of vorticity magnitude.

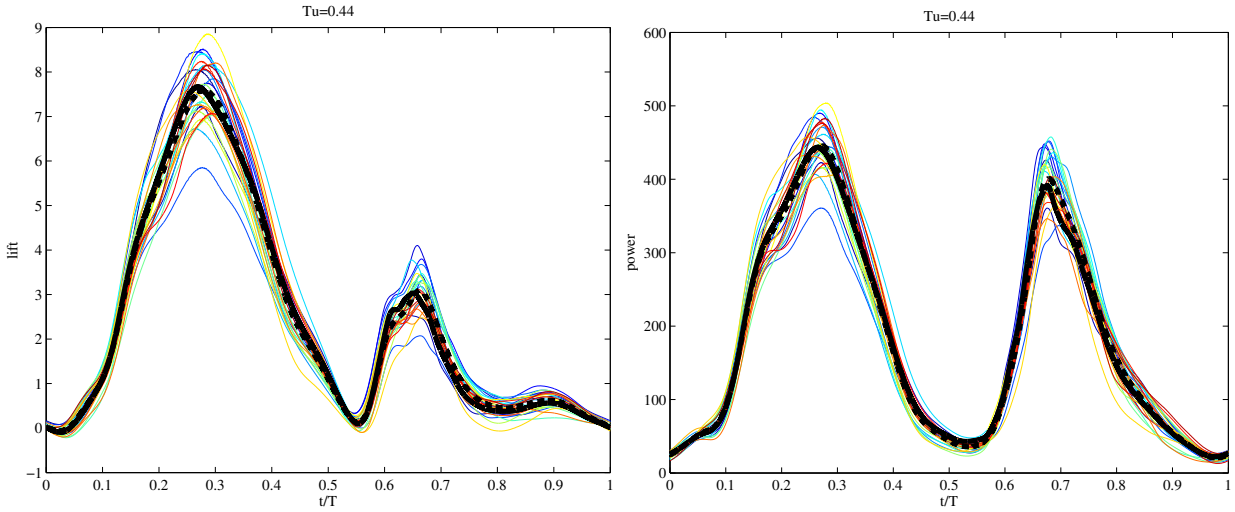

Figure 6. Model housefly. Instantaneous lift force (left) and aerodynamic power (right), both in dimensionless units (using R, f, ϱ_∞ as reference values). The averaged curve (thick black dashed line) and the one of the laminar case (thick black continuous line) almost overlap.

symmetry of the insect. Fig. 7A-B show side and top views of the modeled animal with all linear dimensions normalized to wing length. We numerically computed the inertia tensor, $\underline{\underline{I}}$, of the bumblebee neglecting the wings and assuming uniform body density of $\varrho_b = m/V = 362\,\mathrm{kg/m^3}$, where $V = 0.48\,\mathrm{cm^3}$, from equation

$$\begin{aligned}\underline{\underline{I}} &= \varrho_b \int_V \left((\underline{r}\cdot\underline{r})\,\underline{\underline{E}} - \underline{r}\otimes\underline{r} \right) dV \\ &= \begin{pmatrix} 0.183 & 0 & 0.1307 \\ 0 & 0.400 & 0 \\ 0.1307 & 0 & 0.339 \end{pmatrix}.\end{aligned}$$

Diagonalizing the inertia tensor yields the principal moments of inertia $I_{11} = 0.1092$, $I_{22} = 0.3998$ and $I_{33} = 0.4136$, all in units of $10^{-8}\,\mathrm{kgm^2}$. The data show that moment of inertia about the roll axis (x-axis) is approximately four times smaller than about the yaw and pitch axes, which is in agreement with [13] and [3].

The wing contour was digitized from [1] and the area scaled to $48.37\,\mathrm{mm^2}$ of a single wing and $c = 3.66$ mm mean wing chord (Fig. 7E). Following [16], we modeled wing kinematics from sinusoidal changes in position angle $\phi\,(t/T) = \overline{\phi} + \Phi \sin(2\pi t/T)$ with mean $\overline{\phi} = 24°$ and an amplitude $\Phi = 115°$, using a constant elevation angle $\theta = 12.55°$ with respect to the stroke plane, and assuming a constant feathering angle α of 70° during the upstroke and −40° during the downstroke. At the ventral and dorsal stroke reversal, α changed sinusoidally over a duration of 0.22 cycle durations. The wingbeat kinematics are visualized in Fig. 7D. The inclination angle, η, of the stroke plane against the longitudinal body axis is 37.5°, and the body pitch angle, β is 24.5° with respect to the horizontal plane (Fig. 7C). We modeled the simplified kinematics at an intermediate flight speed of 2.5m/s and a wingbeat frequency f of 152 Hz according to values previously measured in freely flying bumblebees [4, 16]. The modeled wings flapped at mean wing tip velocity of $U = 2\Phi R f = 8.75\,\mathrm{m/s}$ and a Reynolds number of 2042 based on U, c and the kinematic viscosity of air at 300 K, $\nu = 1.57 \cdot 10^{-5}\,\mathrm{m^2/s}$. The fluid density is $\varrho_f = 1.177\,\mathrm{kg/m^3}$.

B. Numerical method

The challenge when simulating insects in turbulence is to accurately resolve a multitude of temporal and spatial scales while taking into account the insect as a complex, time-dependent geometry. To this end, the volume penalization method [2] is employed. Thus we solve the incompressible Navier-Stokes equations,

$$\partial_t \underline{u} + \underline{\omega}\times\underline{u} = -\nabla p + \frac{1}{\mathrm{Re}}\nabla^2\underline{u} - \frac{\chi}{C_\eta}(\underline{u} - \underline{u}_s) \tag{1}$$

$$\nabla\cdot\underline{u} = 0, \tag{2}$$

written in dimensionless form. The penalization term $-\chi/C_\eta\,(\underline{u} - \underline{u}_s)$ has been added to enforce the no-slip boundary condition $\underline{u} = \underline{u}_s$ in the solid. The geometry is encoded in the indicator function χ, which vanishes in the fluid and equals unity in the solid. The penalization parameter is $C_\eta = 2.5 \cdot 10^{-4}$. Since the geometry changes in time, we use a smooth χ-function that is resampled on the Eulerian fluid grid in every time step [6]. Equations (1-2) are solved on an equidistant uniform Cartesian grid of $1152 \times 768 \times 768$ points, using a Fourier pseudospectral discretization [6, 9]. This method is particularly well adapted for turbulence simulations, because of vanishing numerical diffusion and dispersion. The implementation uses highly efficient computational FFT libraries [12], suitable for massively parallel supercomputers. Results presented here are obtained using up to 32768 computing threads on a Blue Gene-Q machine located at IDRIS, Orsay, France. Details about the numerical method and our code for flapping insect flight can be found in [5].

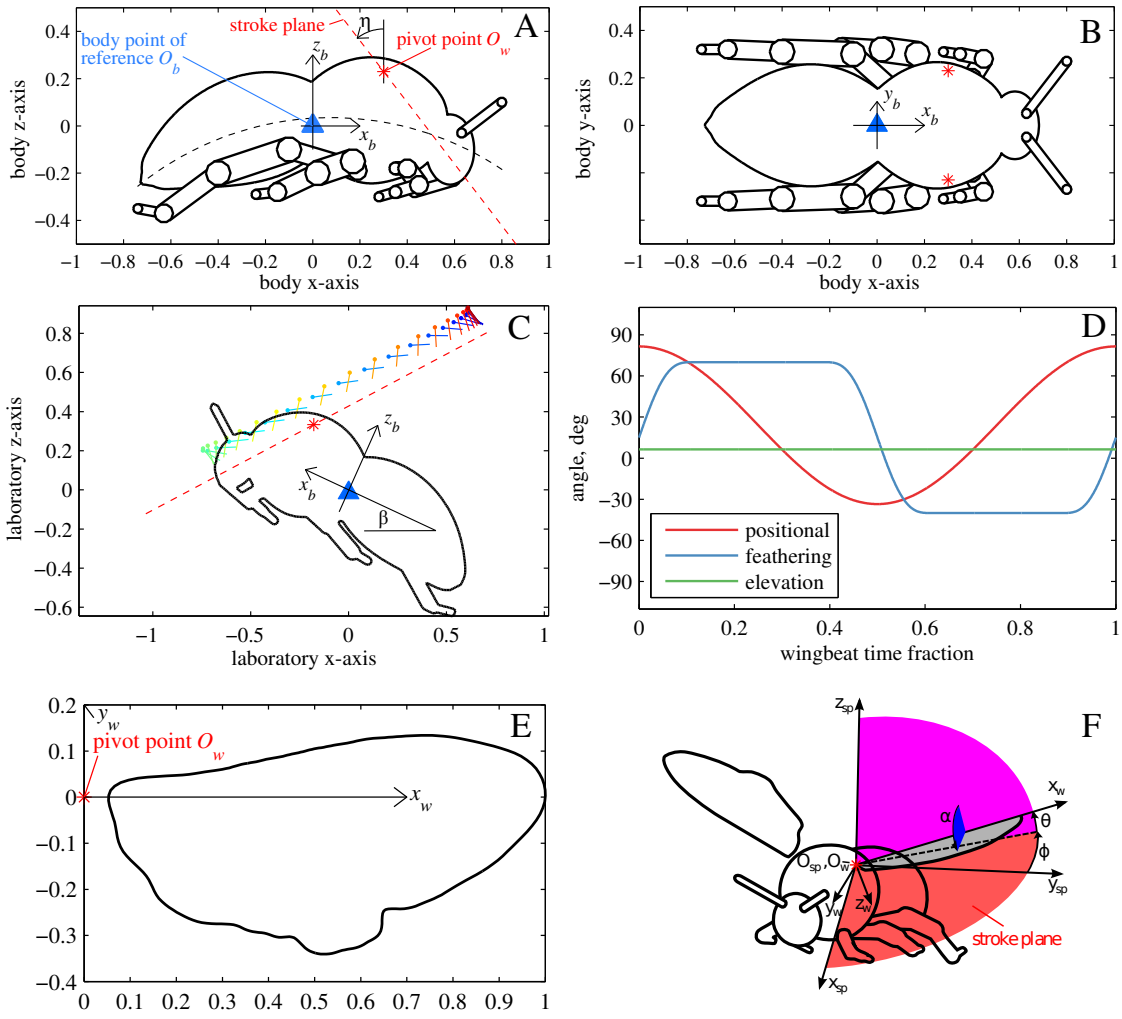

Figure 7. Bumblebee model. (A-B) side and top view of the bumblebee body with the definitions of the body point of reference and the wing pivot points. The body is obtained by sweeping an elliptical section along an arc (black dashed line). The wings rotate around the pivot points (red stars) within the stroke plane, which is inclined by $\eta = 37.5°$ with respect to the body normal. The entire body is inclined by $\beta = 24.5°$ with respect to the horizontal plane (C). The two wings follow the symmetric motion protocol illustrated in D. The wing geometry is shown in E, where the distance pivot point - wing tip is normalized to unity. Wing angles are defined in F.

C. Inflow turbulence

Insects successfully fly in turbulent environments [11, 13, 15]. Since the properties of these aerial perturbations depend on a large number of parameters, we model them by homogeneous isotropic turbulence (HIT). This is a reasonable assumption for the small turbulent scales relevant to insects. The turbulence fields, $\widetilde{\underline{u}}'$, were pre-computed in a periodic computational domain of size $(2\pi)^3$, and we denote quantities from the HIT simulation with the tilde overset. In such a turbulence simulation, we initialized the velocity field at time $\widetilde{t} = 0$ as a random velocity field with given energy spectrum [14]. This velocity field evolved according to the incompressible Navier-Stokes equations, with the energy dissipation compensated by a forcing term [8] that continuously fed energy into the largest fluid scales, i.e., the lowest wavenumbers. After reaching the statistically steady state, independent of the initial condition, we periodically saved snapshots of the velocity field $\widetilde{\underline{u}}'(x, y, z)$.

Different turbulence intensities were computed by modifying the turbulent Reynolds number $R_\lambda = \widetilde{U}\widetilde{\lambda}/\widetilde{\nu}$, where $\widetilde{\lambda}$ is the Taylor-micro scale, defined as $\widetilde{\lambda} = \left(15\widetilde{\nu}\widetilde{U}^2/\widetilde{\varepsilon}\right)^{1/2}$, $\widetilde{U}$ the RMS velocity, $\widetilde{\varepsilon}$ the dissipation rate, and $\widetilde{\nu}$ the dimensionless kinematic viscosity in the HIT simulation. For each value of R_λ, one computation was performed and several snapshots were stored. To ensure that the snapshots are uncorrelated, the saving interval was set to $10\widetilde{T}_0$, where $\widetilde{T}_0$ is the eddy turnover time, $\widetilde{\Lambda}/\widetilde{U}$, and $\widetilde{\Lambda}$ is the integral length scale, $\widetilde{\Lambda} = \frac{\pi}{2\widetilde{U}^2}\int_0^{k_{\max}} k^{-1}\widetilde{E}(k)\,\mathrm{d}k$. This way we generated 44 different turbulence flow fields with parameters assembled in table II of the main article.

The turbulence fields were rescaled to match the normalization of the insect simulations using the relation $\underline{u}' = (2\pi\nu)/(\ell_y\widetilde{\nu})\ \widetilde{\underline{u}}'$ and then added to the imposed mean flow u_∞ in the inlet region of the computational domain (Fig. 8). The scaling relation has one degree of freedom, which is the lateral size of the domain, ℓ_y. Varying ℓ_y is equivalent to changing the animal's size relative to the length scales of the turbulence field. Thus the parameter ℓ_y needs to be large enough to reduce the effect of periodicity in the lateral direction and small enough to produce turbulent length scales similar to natural perturbations. We thus used an intermediate value for the lateral size of $4R$.

D. Numerical wind tunnel

The design of the simulated wind tunnel is illustrated in Fig. 8A-B. At the outlet, a vorticity sponge with a thickness of 48 grid points gradually absorbs the wake to model the appropriate outflow condition [6]. At the inlet, isotropic turbulent fluctuations are added in a slice of 48 grid points thickness to a uniform freestream of 2.5 m/s. The pre-computed turbulence field is imposed by performing a change of variables, $z = u_\infty t/T$. Since the HIT computation is periodic, the injected flow field repeats after $t_{rep} = \ell_y/u_\infty = 3.21T$. The initial condition corresponds to unperturbed laminar flow, thus the turbulent–laminar interface travels downstream, as illustrated in Fig. 8A, and turbulence hits the head and tail of the model bumblebee approximately after 0.95 and 2 wing strokes, respectively. Throughout the remaining computational sequence, the insect is entirely immersed in the turbulent flow. Owing to laminar flow conditions, we thus excluded the first two wing strokes of each simulation from the statistical analysis.

Each simulation run was repeated N_R times (table II of main article) and yielded four subsequent, uncorrelated wing strokes. The simulation stopped after six wing strokes because the following strokes are no longer independent owing to the repetition of the imposed inflow perturbation. This procedure guaranteed confident statistical means and variances of aerodynamic forces and power. It also ensured that the results were not biased by a randomly present coherent structure in the turbulent inflow field.

E. Wake turbulence in laminar inflow

Figure 9 and Movie S1 illustrate the wake generated by the bumblebee without upstream perturbations.

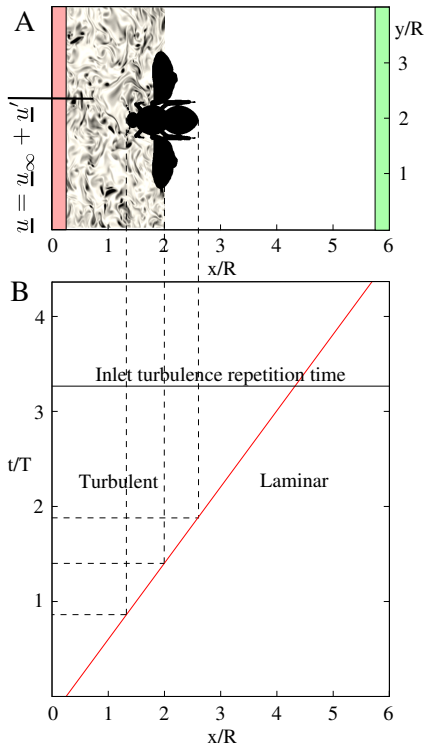

Figure 8. Sketch of the computational setup with the insect tethered at $x/R = 2$. The red shaded area indicates where the inflow, consisting of a uniform mean flow and turbulent fluctuations, $\underline{u} = \underline{u}_\infty + \underline{u}'$, is imposed. The green area is the outflow vorticity sponge [6]. (B) Propagation of the turbulent front (red line) in the space-time diagram. The inflow turbulence $\underline{u}'$ field repeats after $t/T = 3.21$.

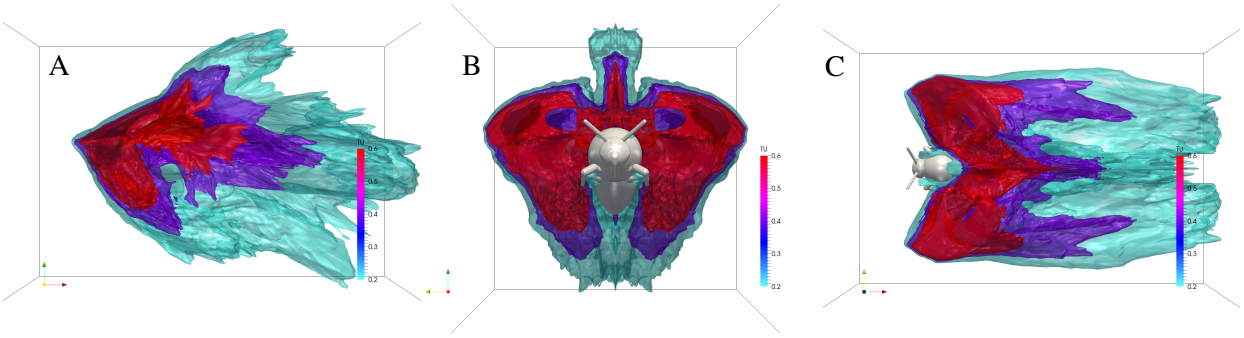

Figure 9. Wake generated by the bumblebee under laminar inflow conditions, illustrated by the $\{0.2, 0.4, 0.6\}$ isosurfaces of $Tu = \sqrt{2\overline{u'^2}/3}/u_\infty$. The mean turbulent kinetic energy is computed as $\overline{u'^2} = \left(\overline{u^2} - \overline{u}^2\right)$.

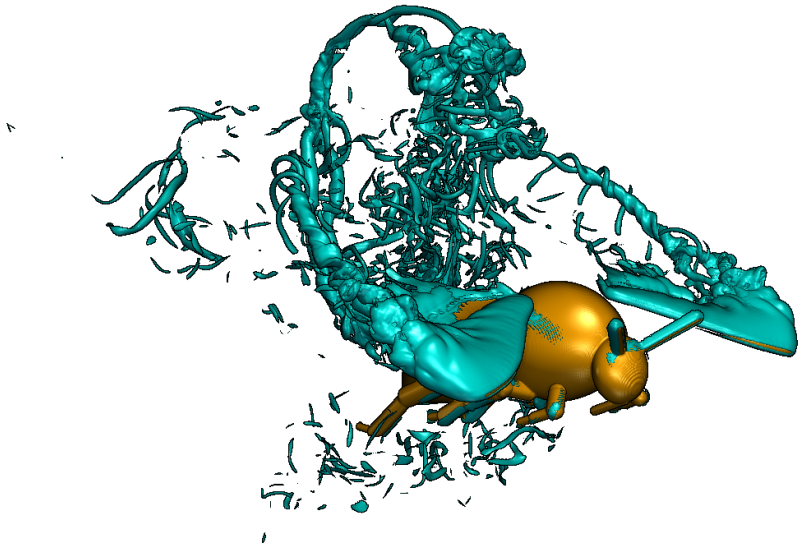

Movie S1. Wake generated by the bumblebee under laminar inflow conditions, illustrated by the $\|\underline{\omega}\| = 100$ isosurface of vorticity magnitude.

[1] University of Minnesota Insect Collection. http://insectcollection.umn.edu. Accessed: 2014-05-14.

[2] P. Angot, C. Bruneau, and P. Fabrie. A penalization method to take into account obstacles in incompressible viscous flows. *Numer. Math.*, 81:497–520, 1999.

[3] S. A. Combes and R. Dudley. Turbulence-driven instabilities limit insect flight performance. *Proc. Natl. Acad. Sci. USA*, 106:9105–9108, 2009.

[4] R. Dudley and C. P. Ellington. Mechanics of forward flight in bumblebees I. kinematics and morphology. *J. Exp. Biol.*, 148:19–52, 1990.

[5] T. Engels, D. Kolomenskiy, K. Schneider, and J. Sesterhenn. FluSI: A novel parallel simulation tool for flapping insect flight using a Fourier method with volume penalization. *arXiv:1506.06513, SIAM J. Sci. Comput., under revision*, 2015.

[6] T. Engels, D. Kolomenskiy, K. Schneider, and J. Sesterhenn. Numerical simulation of fluid-structure interaction with the volume penalization method. *J. Comput. Phys.*, 281:96–115, 2015.

[7] S. N. Fry, R. Sayaman, and M .H. Dickinson. The aerodynamics of hovering flight in Drosophila. *J. Exp. Biol.*, 208(Pt 12):2303–18, June 2005.

[8] Y. Kaneda, T. Ishihara, M. Yokokawa, K. Itakura, and A. Uno. Energy dissipation rate and energy spectrum in high resolution direct numerical simulations of turbulence in a periodic box. *Phys. Fluids*, 15(2):L21–L24, 2003.

[9] D. Kolomenskiy, H. K. Moffatt, M. Farge, and K. Schneider. Two- and three-dimensional numerical simulations of the clap-fling-sweep of hovering insects. *J. Fluids Struct.*, 27:784–791, 2011.

[10] M. Maeda and H. Liu. Ground effect in fruit fly hovering: A three-dimensional computational study. *J. Biomech. Sc. Engin.*, 8:344–355, 2013.

[11] V. M. Ortega-Jimenez, J. S. M. Greeter, R. Mittal, and T. L. Hedrick. Hawkmoth flight stability in turbulent vortex streets. *J. Exp. Biol.*, 216:4567–4579, 2013.

[12] D. Pekurovsky. P3DFFT: a framework for parallel computations of Fourier transforms in three dimensions. *SIAM J. Sci. Computing*, 34:C192–C209, 2012.

[13] S. Ravi, J.D. Crall, A. Fisher, and S. A. Combes. Rolling with the flow: bumblebees flying in unsteady wakes. *J. Exp. Biol.*, 216:4299–4309, 2013.

[14] R. S. Rogallo. Numerical experiments in homogeneous turbulence. *NASA Technical Memorandum*, 81315:1–93, 1981.

[15] J. T. Vance, I. Faruque, and J. S. Humbert. Kinematic strategies for mitigating gust perturbations in insects. *Bioinspir. Biomim.*, 8(1):016004, 2013.

[16] N. Xu and M. Sun. Lateral dynamic flight stability of a model bumblebee in hovering and forward flight. *J. Theor. Biol.*, 319:102–115, 2013.